

Normalizing Flow to Augmented Posterior: Conditional Density Estimation with Interpretable Dimension Reduction for High Dimensional Data

Cheng Zeng^{*} George Michailidis[†] Hitoshi Iyatomi[‡] Leo L Duan[§]

July 8, 2025

Abstract

The conditional density characterizes the distribution of a response variable y given other predictor x , and plays a key role in many statistical tasks, including classification and outlier detection. Although there has been abundant work on the problem of Conditional Density Estimation (CDE) for a low-dimensional response in the presence of a high-dimensional predictor, little work has been done for a high-dimensional response such as images. The promising performance of normalizing flow (NF) neural networks in unconditional density estimation acts a motivating starting point. In this work, we extend NF neural networks when external x is present. Specifically, they use the NF to parameterize a one-to-one transform between a high-dimensional y and a latent z that comprises two components $[z_P, z_N]$. The z_P component is a low-dimensional subvector obtained from the posterior distribution of an elementary predictive model for x , such as logistic/linear regression. The z_N component is a high-dimensional independent Gaussian vector, which explains the variations in y not or less related to x . Unlike existing CDE methods, the proposed approach, coined Augmented Posterior CDE (AP-CDE), only requires a simple modification on the common normalizing flow framework, while significantly improving the interpretation of the latent component, since z_P represents a supervised dimension reduction. In image analytics applications, AP-CDE shows good separation of x -related variations due to factors such as lighting condition and subject id, from the other random variations. Further, the experiments show that an unconditional NF neural network, based on an unsupervised model of z , such as Gaussian mixture, fails to generate interpretable results.

Keywords: Conditional density estimation; Image generation; Normalizing flow; Supervised dimension reduction.

^{*}Department of Statistics, University of Florida, U.S.A. czeng1@ufl.edu

[†]Department of Statistics and Data Science, University of California Los Angeles, U.S.A. gmichail@ucla.edu

[‡]Department of Applied Informatics, Graduate School of Science and Engineering, Hosei University, Japan. iyatomi@hosei.ac.jp

[§]Corresponding author. Department of Statistics, University of Florida, U.S.A. li.duan@ufl.edu

1 Introduction

A conditional density characterizes the probabilistic behavior of a set of random variables, when information on a set of other variables is available. The case of a single variable y (the response) conditioned on a multivariate x (predictor) has received most attention in the literature, due to a wide range of applications. A number of methods have been proposed to address the conditional density estimation (CDE) problem from observed data. Kernel density (Terrell and Scott, 1992; Botev et al., 2010; Kim and Scott, 2012) and k-nearest neighbors (Mack and Rosenblatt, 1979; Kung et al., 2012) based techniques have been extensively studied and employed in applications. Another popular approach uses a mixture model of the form $f(y_i | x_i) = \sum_{k=1}^K w_k(x_i)g(y_i | \theta_k(x_i))$ over data index $i = 1, \dots, n$, with $\sum_{k=1}^K w_k(x_i) = 1$ and potentially $K \rightarrow \infty$. In the mixture model and for continuous y_i , $g(\cdot)$ can be a location-scale density, such as a multivariate Gaussian one with mean μ_k and covariance matrix Σ_k . Importantly, the mixture component parameters θ_k as well as the mixture weights w_k are some deterministic transforms of the x_i 's, hence allowing the mixture distribution of y_i to vary according to x_i . There is a large literature in such a framework, see, e.g., Jiang and Tanner (1999); Geweke and Keane (2007); Villani et al. (2009); Norets (2010); Huang et al. (2022) and references therein.

The CDE framework has a wide range of statistical applications, besides serving as a nonlinear predictive model for y_i , including outlier detection and classification. In the first case, by evaluating the magnitude of $f(y_i | x_i)$ for each observed data point, one could identify those points in the bottom density quantile as potential outliers (Scott, 2004; Schubert et al., 2014). In the latter case, when x_i is a discrete class label, such as whether a patient is in disease status, with a class probability $p(x_i)$, $p(x_i | y_i) \propto p(x_i)f(y_i | x_i)$ could be used as a probabilistic classifier for predicting x_i (Garg and Roth, 2001).

Despite significant advances in CDE, in recent years, a number of major challenges are not satisfactorily addressed for a high-dimensional response $y_i \in \mathbb{R}^p$, such as an image. Hence, the focus of the current work is on the case of a high-dimensional response y_i —rather than low-dimensional response conditioned on a high-dimensional predictor x_i in extant literature. For the latter, a large class of solutions exist, such as BART (Chipman et al., 2010), that partition the high-dimensional space of x_i and use simple piece-wise distribution (such as spherical Gaussian, or Bernoulli) for the low-dimensional y_i in each region. Obviously, this strategy does not be applied to high-dimensional y_i .

When using the mixture models for density estimation, the following two difficulties arise for a high-dimensional data y : (i) specification of the component distribution g in the mixture model and (ii) the curse of dimensionality when computing a high-dimensional mixture distribution. These two points are elaborated next. First, a parametric specification of the component distribution g can be unsatisfactory, since location-scale distribution is often an over-simplification for high-dimensional data. For example, for a collection of face photos from one subject, the mean of a Gaussian density g is often a poor summary characterization for this group of data points, since there are other factors (such as unknown lighting condi-

tions) that contribute to the within-group variability, besides just pixel-wise random noise. To address this issue, it is often useful to assume that the high-dimensional data point lie close to several manifolds, each having an intrinsic low dimension. One of the well-known solutions is the mixture of factor analyzers (MFA) (McLachlan and Peel, 2000; Tang et al., 2012), or mixture of probabilistic principal component analysis (PCA) (Tipping and Bishop, 1999), which retains the multivariate Gaussian density $g(y_i | \mu_k(x_i), \Sigma_k)$; further, the covariance matrix takes the form $\Sigma_k = U_k U_k' + \Lambda_k$, with U_k some $p \times d$ matrix with d small, and Λ_k a diagonal positive matrix. Effectively this parameterization assumes that for some h , $y_i - \mu_k(x_i)$ lies near a linear subspace spanned by the columns of U_k . However, it is rather difficult to extend this technique to non-linear manifolds through non-linear mappings. Alternatively, a popular idea is to find a low-dimensional representation, or “embeddings” that preserve some (often not all) relational characteristics of the high-dimensional data, such as pairwise distances or local neighborhoods. Such embedding is denoted by $z_i \in \mathbb{R}^d$ for each data point. Examples include Sammon’s mapping (Sammon, 1969), kernel PCA (Schölkopf et al., 1997), Laplacian eigenmaps (Belkin and Niyogi, 2003), locally-linear embeddings (Roweis and Saul, 2000), Gaussian process latent variables (GPLV) (Lawrence, 2003), t-distributed stochastic neighbor embeddings (t-SNE) (Van der Maaten and Hinton, 2008), uniform manifold approximation and projection (UMAP) (McInnes et al., 2018), just to name a few. After obtaining such z_i ’s, one could calculate the conditional density $f(z_i | x_i)$ for z_i , as a surrogate the corresponding conditional density for y_i . Despite some success in visualization tasks and cluster analysis, a key issue among the aforementioned methods is that the procedure of dimension reduction often lacks a generative distribution (except for GPLV); consequently, a density for $f(y_i | x_i)$ can not be obtained.

The second difficulty is the curse of dimensionality when computing a high-dimensional mixture distribution, which is often overlooked in the literature. Common algorithms used for mixture model estimation involve a discrete latent variable $z_i = h$ with probability w_k , given that $(y_i | z_i = h, x_i)$ comes from a component distribution $g(\cdot | \theta_k(x_i))$. Since $p(z_i = h | y_i, \theta_k) \propto w_k f(y_i | \theta_k(x_i))$, it allows iterating through the following two steps: (a) sampling of z_i via a multinomial distribution (or taking expectation $\tilde{z}_i = p(z_i = h | y_i, \theta_k)$ in the EM algorithm (Fraley and Raftery, 2002)); (ii) updating $\theta_k(x_i)$ conditioned on z_i or \tilde{z}_i . Nevertheless, since for $h = 1, \dots, K$, the high-dimensional y_i creates large magnitude of densities, thus resulting in $f(y_i | \theta_k(x_i)) / f(y_i | \theta_l(x_i)) \approx 0$ or ∞ , unless $\theta_k(x_i) \approx \theta_l(x_i)$. Consequently, each $p(z_i | y_i, \theta_k(x_i))$ is very likely to be stuck at 1 for a given h^* , and close to 0 for all the other $h \neq h^*$, with the end result being that the estimation algorithm “gets stuck” at the initial assignment z_i ’s.

The curse-of-dimensionality for density estimation is a well known issue and the reason that algorithms such as rejection sampling, importance sampling, and Metropolis-Hastings fail in high dimensions (Gelfand, 2000; Zuev et al., 2011). A similar problem was recently discovered in high-dimensional clustering (Chandra et al., 2023), which is closely related to the unconditional density estimation problem.

These challenges in high-dimensional density estimation approaches motivated the de-

velopment of completely different approaches. Normalizing flow neural networks were proposed to find an invertible mapping between a random variable $y_i \in \mathbb{R}^p$ and a latent variable $z_i \sim N(0, I_p)$. The neural network is formed by stacking layers of non-linear transforms, each layer parameterized in the way such that it corresponds to a bijective transform, and the inverse transform has a closed-form or can be computed efficiently. Using a simple change-of-variable technique, one could obtain the density $f(y_i)$ as a transformed density from an independent Gaussian one. Examples include RealNVP (Dinh et al., 2016), MADE (Germain et al., 2015), MAF (Papamakarios et al., 2017), Glow (Kingma and Dhariwal, 2018), FFLORD (Grathwohl et al., 2018) and iResNet (Behrmann et al., 2019; Chen et al., 2019). Due to the large number of parameters and expressiveness of neural networks, impressive performance has been exhibited as a generative model for y_i . For example, in image applications, after training a normalizing flow network, one could generate a new Gaussian vector $z_{i'}$ and push it forward through the trained network, with the transformed $y_{i'}$ often looking as if it were a real photo. Since there is only one neural network involved (despite a large number of parameters within it), the computation enjoys high efficiency through stochastic gradient descent. Its expressiveness as a generative model, tractability of the target density $f(y_i)$ and good computing performance make the normalizing flow a compelling alternative to mixture models for high-dimensional density estimation provided the training data set is large enough.

On the other hand, since one can inversely obtain z_i as a deterministic transform of y_i , a number of interesting directions of exploration for z_i arise. One of them is whether a more interpretable modeling structure for z_i can be used, other than just being drawn from an independent Gaussian distribution. Early examples includes using a mixture of Gaussian distribution (Izmailov et al., 2020), or a mixture of subspace structure (Peng et al., 2020) to name a select few. Although some interpretable results, including improved clustering accuracy were reported, it was later discovered that most of the improved results were largely due to the specific pre-processing of the reported data sets (Haeffele et al., 2020), instead of the selected distribution for z_i . This cautionary tale serves as a good warning, that it is quite difficult—if not impossible—to rely on unsupervised normalizing flow (that is, using y_i alone) to find structure in the latent z_i . Naturally, this motivates us to consider external information from x_i , and create a normalizing flow-based conditional density estimator.

The focus is on the CDE problem involving a high-dimensional y_i and low-dimensional x_i ; for example, x_i could correspond to labels, or a continuous vector providing context information for the observed y_i . Specifically, we use the normalizing flow to form an invertible transform of data y_i and an “augmented posterior (AP)” based z_i that comprises of two components $[z_{P,i}, z_{N,i}]$; $z_{P,i}$ is a low-dimensional subvector that forms a joint distribution with x_i , such as via simple logistic/linear regression likelihood $f(x_i | z_{P,i})$. Effectively, the distribution of $[z_{P,i}, z_{N,i}]$ is the posterior distribution of $(z_{P,i} | x_i)$ augmented by independent Gaussian $z_{N,i}$. Note that there has been some recent work on normalizing flow based CDE, e.g., Papamakarios et al. (2017). However, the proposed approach enjoys several

unique advantages: first, it produces a supervised dimension reduction in those $z_{P,i}$ within the CDE framework; second, it requires only simple modification of the common normalizing flow networks, so it is very easy to implement; last, it produces a single latent variable z_i for each data point y_i , and hence the unconditional density calculation does not involve summation or integration over the space of the predictor variable. We will illustrate these advantages as well as the outperformed density estimation results in this article.

2 Preliminary: Generative Models based on Normalizing Flows

This section provides some preliminary on the normalizing flow neural networks. Suppose there is a one-to-one and differentiable almost everywhere mapping $T_\theta : \mathbb{R}^p \rightarrow \mathbb{R}^p$ (with θ the parameters within it), that can transform random variable y into another latent continuous $z \in \mathbb{R}^p$ following a simple distribution f_z . With a slight abuse of notation, f is used to represent both a density and a probability function. After a change of variable, for $i = 1, \dots, n$:

$$f_y(y_i) = f_z[T_\theta(y_i)]|\nabla_y T_\theta(y_i)|,$$

with $|\nabla_y T_\theta(\cdot)|$ being the determinant of the Jacobian matrix with the gradient taken with respect to y_i . To estimate T_θ , one typically minimizes the Kullback–Leibler (KL) divergence between the target distribution $f_y^*(y)$ and the normalizing flow-based $f_y(y)$, which is

$$\text{KL}[f_y^*(y), f_z[T_\theta(y)]|\nabla_y T_\theta(y)|] \approx \frac{1}{n} \sum_{i=1}^n \{-\log f_z[T_\theta(y_i)]|\nabla_y T_\theta(y_i)|\} + \text{constant},$$

where the right hand side is the empirical KL, equaling to the loss function to be minimized over θ .

To flexibly parameterize the transform while maintaining invertibility, one uses a special multilayer neural network (“invertible neural network”) with $T = T_1 \circ T_2 \circ \dots \circ T_m$, and each $T_k : \mathbb{R}^p \rightarrow \mathbb{R}^p$ is a layer of an invertible transform of relatively simple operations; for example, in RealNVP (Dinh et al., 2016), the input of T_k is equally partitioned to $r = [r_A, r_B]$, and $T_k([r_A, r_B]) = [r_A, r_B \odot s(r_A) + l(r_A)]$, with s and l functions that produce the location-scale change to r_B . Then in the next layer, one alternates by using $T_{k+1}([r_A, r_B]) = [r_A \odot s(r_B) + l(r_B), r_B]$. Other types of neural networks include autoregressive flows and residual flows. We refer readers to Papamakarios et al. (2021) as a review for all types of flows employed. Besides invertibility, these neural networks are also carefully designed so that the term of the determinant of the Jacobian and the inverse mapping of the neural networks can be computed at low cost.

Obtaining an approximate solution of T_θ via an invertible neural network leads to a transport map $T_{\hat{\theta}}$, that gives a density estimator for the data $\hat{f}_y(y_i) = f_z[T_{\hat{\theta}}(y_i)]|\nabla_y T_{\hat{\theta}}(y_i)|$. This method is commonly referred to as “normalizing flow”, since one often assigns a standard independent Gaussian distribution to $z \sim N(0, I_p)$ for simplicity, which is often called

the base distribution. As a generative model, one can sample $z_{i'} \sim \mathcal{N}(0, I_p)$, and then $y_{i'} = T_{\hat{\theta}}^{-1}(z_{i'})$ produces new generated data from the estimated distribution f_y .

3 Method

The section begins by introducing notation used in the sequel. Let $y_i \in \mathbb{R}^p$ be a continuous response with distribution f_y , and $x_i \in \mathcal{X} \subseteq \mathbb{R}^m$ be the corresponding predictor variable (could be discrete, continuous, or a mix of both) drawn from another distribution f_x . We focus on the case of large p and small m .

3.1 Augmented Posterior for CDE

To enable CDE for $f_{y|x}(y_i | x_i)$, as well as making the latent variable z_i more interpretable, we consider a joint distribution between z and x ,

$$f_{z,x}(z_i, x_i) = f_{z_N}(z_{N,i})f_{z_P}(z_{P,i})f_{x|z}(x_i | z_{P,i}; \beta), \quad (1)$$

independently for $i = 1, \dots, n$, where $z_i = [z_{P,i}, z_{N,i}]$. The first component $z_{P,i} \in \mathbb{R}^d$ is a low-dimensional subvector and is used in a predictive model for x_i , whereas the second component $z_{N,i} \in \mathbb{R}^{p-d}$ is a high-dimensional subvector unrelated to x_i , and β is viewed as a non-random parameter that will be estimated. If one considers $f_{x|z}$ to be the likelihood for x , and f_z to be the prior distribution for z , then it is not hard to see that,

$$f_{z|x}(z_i | x_i) = f_{z_N}(z_{N,i}) \frac{f_{z_P}(z_{P,i})f_{x|z}(x_i | z_{P,i}; \beta)}{\int_{\mathbb{R}^d} f_{z_P}(t)f_{x|z}(x_i | t; \beta)dt},$$

where the second part is the posterior of z_P , $f_{z_P|x}(z_{P,i} | x_i; \beta)$, and $f_{z_N}(z_{N,i})$ is an independent random variable that augments this posterior, to make z_i match the dimension of y_i . Therefore, each $z_i = (z_{P,i}, z_{N,i})$ is referred to as a sample point from an *augmented posterior*.

Figure 1 shows the architecture of the proposed model. Note that for simplicity, we retain the standard independent Gaussian density for f_{z_N} and f_{z_P} as in a typical normalizing flow, while employing a generalized linear model for $f_{x|z}$. For example, if $x_i \in \mathbb{R}^m$ is continuous, then one can use $x_i = \beta_0 + \beta_1 z_i + \epsilon_i$, with $\beta_0 \in \mathbb{R}^m$, β_1 an $m \times d$ matrix, and $\epsilon_i \stackrel{iid}{\sim} \mathcal{N}(\vec{0}, \text{diag}(\beta_2))$ with β_2 positive vector. For each univariate discrete $x_{i,j} \in \{1, \dots, K\}$, one can use a multinomial logistic regression in $f_{x|z}$, $p(x_{i,j} = k | z_{P,i}) \propto \exp(\beta_{0,k} + \beta'_k z_{P,i})$, with $\beta_{0,k} \in \mathbb{R}$, $\beta_k \in \mathbb{R}^d$ for $k = 1, \dots, K-1$, and β_K and $\beta_{0,K}$ fixed to 0-value as common in logistic regression. In general, the conditional probability function $f_{x|z}$ could be proportional to the original function to the power λ for the purpose of regularization. This is commonly used in robust Bayesian models (Grünwald and Van Ommen, 2017) and hybrid deep generative models (Nalisnick et al., 2019). In the proposed model, the normalizing constant is merged into the denominator of the posterior $f_{z_P|x}$ naturally, and the model is still a generative one.

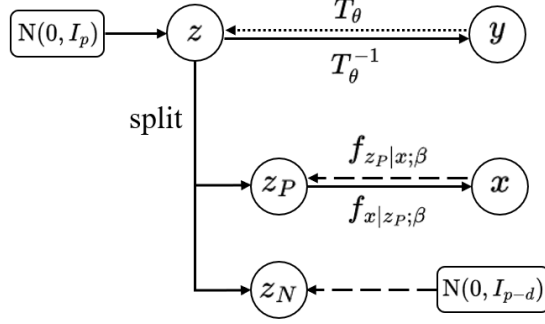


Figure 1: The diagram of the architecture of AP-CDE. The solid lines show the generative process for the data (y, x) . The dashed lines show how to generate a new latent variable z from the augmented posterior.

In the case of x_i having both continuous and (potentially more than one) discrete elements, $x_i = [x_{A,i}, x_{B,i}]$, one can partition $z_{P,i} = [z_{P_A,i}, z_{P_B,i}]$, and use a separable likelihood function $f_{x|z_P}(x_i | z_{P,i}) = f_{x_A|z_{P_A}}(x_{A,i} | z_{P_A,i})f_{x_B|z_{P_B}}(x_{B,i} | z_{P_B,i})$ —where the first term on the right models the continuous part, and the second term does the discrete part. This separation in z_P is motivated by applications under consideration, in which commonly the discrete part corresponds to the class label of an image, whereas the continuous part to other conditions (such as lighting) that are unrelated to the labeling information.

Next, if there is an invertible mapping T_θ that connects z_i and y_i , by applying change-of-variable, one has

$$f_{y|x}(y_i | x_i) = f_{z|x}[T_\theta(y_i) | x_i; \beta] |\nabla_y T_\theta(y_i)|.$$

To estimate this mapping T_θ as well as the parameter β in the predictive model of x_i , one minimizes the empirical KL divergence between the target distribution $f_{y|x}^*(y | x)$ and the $f_{y|x}(y | x)$ in the above, leading to:

$$\min_{\theta, \beta} \frac{1}{n} \sum_{i=1}^n \left\{ -\log f_z[T_\theta(y_i)] |\nabla_y T_\theta(y_i)| - \log f_{x|z}[x_i | T_\theta^P(y_i); \beta] + \log \int_{\mathbb{R}^d} f_{z_P}(t) f_{x|z}(x_i | t; \beta) dt \right\}, \quad (2)$$

where $T_\theta^P(z_i)$ [or, $T_\theta^N(z_i)$] means taking the subvector (corresponding to z_P , or z_N) from the output of $T_\theta(z_i)$. Although the last integral above is often intractable, as the stochastic gradient descent technique (the commonly used optimization algorithm in normalizing flow) only requires an approximate gradient via taking a random subset of size n_b instead of n , one can replace the last term via a Monte Carlo estimate, $\log [\sum_{l=1}^M f_{x|z}(x_i | t_l; \beta) / M]$, with each $t_l \stackrel{iid}{\sim} f_{z_P}$ [in this article, $N(\vec{0}, I_d)$]. The n_b integrals to be estimated can share those M random samples t_l 's across i in the subset of size n_b , and hence the estimation is inexpensive.

After the KL divergence is minimized, a conditional density estimator is obtained by

$$\hat{f}_{y|x}(y_i | x_i) = f_{z|x}[T_{\hat{\theta}}(y_i) | x_i; \hat{\beta}] |\nabla_y T_{\hat{\theta}}(y_i)|.$$

Further, to calculate the marginal density of y for a new data point for which only the response y_i is available, one can simply marginalize over x_i in Equation (1), and obtain

$$f_y(y_i) = f_{z_N}[T_{\hat{\theta}}^N(y_i)] f_{z_P}[T_{\hat{\theta}}^P(y_i)] |\nabla_y T_{\hat{\theta}}(y_i)|.$$

Therefore, after the optimization, both conditional and marginal density estimation can be accomplished in a computational efficient manner.

3.2 Supervised Dimension Reduction and Validation

Besides conditional density estimates, another advantage of using the augmented posterior is that it produces a low-dimensional representation $z_{P,i}$ that is related to the variations in x_i . Indeed, after the optimization step concludes, one obtains a computational form that produces low-dimensional $z_{P,i} = T_{\hat{\theta}}^P(y_i)$, and $T_{\hat{\theta}}^P$ is estimated under supervising information from x .

On the other hand, one may further wonder if $z_{P,i}$ has captured all the useful information that connects y_i and x_i . To formalize, if the true data generating mechanism for (y_i, x_i) is indeed based on $z_i \sim f_z$, $y_i = T_{\theta}^{-1}(z_i)$, $x_i \sim f_{x|z_P}$, then one would have the following sufficient dimension reduction outcome:

$$x \perp\!\!\!\perp y | T_{\theta}^P(y),$$

as the ideal result.

There are ways to test conditional independence in classical linear models (Cook and Ni, 2005) and non-linear low dimensional models (Su and White, 2007, 2008). However, the combination of nonlinearity and high dimensionality poses significant challenges. Fortunately, for high-dimensional data with y_i and x_i , this can be validated via synthesizing new data and predicting x_i via another neural network G , independently trained with (y_i, x_i) 's.

Specifically, for each $z_i = T_{\hat{\theta}}(y_i)$ produced, one fixes $z_{P,i}$ while replacing $z_{N,i}$ with an independently sampled $\tilde{z}_{N,i,j} \sim \mathcal{N}(0, I_{p-d})$ for $j = 1, \dots, J$. Then synthesized $\tilde{y}_{i,j} = T_{\hat{\theta}}^{-1}[z_{P,i}, \tilde{z}_{N,i,j}]$ is obtained. One predicts the x_i using $\tilde{y}_{i,j}$ via the separately trained network G , and observes if each predicted $\hat{x}_{i,j}$ differ from the observed x_i —in the ideal case, $\hat{x}_{i,j}$ should not differ much from x_i (since $z_{P,i}$ should contain most of the predictive information about x_i), and the conditional independence can be quantified by the error rate.

3.3 Parameterization Details

In this article, T_{θ} is parameterized using the state-of-art normalizing flow Glow (Kingma and Dhariwal, 2018). We choose Glow in the experiments for its high accuracy on the density estimation and the ease of implementation. It employs a multi-scale architecture

(Dinh et al., 2016), which contains L levels. After each level, half of the dimensions of latent z_i are immediately modeled as Gaussians, while the remaining half are further transformed by the flows. This significantly improves the computation efficiency. Each level consists of K (depth) steps of flow that share an identical structure which contains an activation normalization, an invertible 1×1 convolution and an affine coupling layer. In this article, we use the additive coupling layer as a special case of the affine coupling layer, in which the number of channels of the hidden layers (convolutional neural networks) is set to be 512.

Under this kind of multi-scale architecture, the following important problem is how to choose the way of splitting z_i into $[z_{P,i}, z_{N,i}]$. First, to make the Monte Carlo estimation of the integral in Equation (2) accurate, efficient and stable, one does not expect d , the dimension of $z_{P,i}$, too large. Second, since the outputs from the later layers experience more transforms compared to the ones from the earlier layers, choosing dimensions of $z_{P,i}$ from the relatively later layers will improve the model performance. This is illustrated in the numerical experiments.

4 Numerical Experiments

The following set of numerical experiments demonstrates the AP-CDE’s advantages for density estimation and dimensional reduction. The following competing models are used to compare its performance: (i) the Glow normalizing flow based on independent Gaussian $z \sim N(\vec{0}, I_p)$, without using any information from x ; (ii) a modified Glow based on a Gaussian mixture (named Glow-Mix), $z_i \sim \sum_{k=1}^K w_k N(\mu_k, I_p)$, with K set to the ground-truth number of classes in the data; and (iii) a CDE extended from Glow (named Glow-CDE) by adding x_i as an input in each additive coupling layer (Papamakarios et al., 2017, Section 3.4). When the predictor variable x_i is discrete, e.g., class label, the comparison is also made with (iv) a naive CDE model based on Glow where for each value x' of x_i a Glow is trained on those data y_i with $x_i = x'$ (named Glow-NCDE). For a fair comparison, we set the four competitors to have the same numbers of levels L and the same depth K , as in the AP-CDE model. The first two models perform unconditional density estimation with producing latent variables, whereas the last two models are conditional. Unlike the proposed model, the two CDE models compared do not have a unique corresponding latent variable for a new data. Note that the fourth model is inefficient because one has to train models of number of classes of x .

We use the Adam optimizer (Kingma and Ba, 2014) provided in the PyTorch framework to train all models, with a mini batch size of $n_b = 64$ and learning rate at 0.0005 for all models. All models are trained for 200 epochs, where the optimizer goes through the whole training dataset exactly once in each epoch. For the first 10 epochs as warm-up, the learning rate linearly increases to 0.0005 after each batch training. Then the learning rate goes down to 10^{-4} using cosine annealing schedule (Loshchilov and Hutter, 2016). We monitor the loss function of all models and ensure that convergence is achieved by all models. Finally, $M = 1000$ is set in the Monte Carlo estimator for the integral in Equation (2).

The experiments are based on the following two datasets: the FashionMNIST one of the fashion products (Xiao et al., 2017) and the Extended Yale Face B one of face images (Lee et al., 2005). These images have a single color channel, containing pixel values $\{0, \dots, 255\}$. We follow Papamakarios et al. (2017); Dinh et al. (2016) to dequantize the pixel values by adding standard uniform noise onto every pixel and scaling the values to $(0, 1)$ by dividing 256. Additional numerical experiments are shown in the Appendix A.

4.1 FashionMNIST Images of Fashion Products

The FashionMNIST data is used to illustrate the CDE when x_i is discrete. This dataset contains 70,000 processed images of fashion products, each having 28×28 pixels. Among them, 60,000 is used for training purposes and the remaining is used for testing. Each image y_i is associated with a discrete label x_i with values from 0 to 9 recording the ground-truth fashion products, including T-shirt, sandal, bag, etc. Each image is padded to dimension 32×32 by adding 2 more dimensions of 0 in each of four direction, and then extend each image to 3 channels by repeating the image in each of channel.

For the Glow model, levels $L = 3$ and depth $K = 32$ are set. For the sub-model $f_{x|z}$ in AP-CDE, we use the likelihood function of the multinomial logistic regression, as stated in Section 3.1. Since the labels are relatively balanced across classes, to improve interpretation on the latent $z_{P,i}$'s, all intercept terms $\beta_{0,k}$'s are set to be zeros. We compare several choices of the dimensions of $z_{P,i}$. To be clear, in the multi-scale architecture, when the data y_i has dimension $3 \times 32 \times 32$, the output $z_i^{(1)}$ from the first level has dimension $6 \times 16 \times 16$, the output $z_i^{(2)}$ from the second level has dimension $12 \times 8 \times 8$, while the final output $z_i^{(3)}$ has dimension $48 \times 4 \times 4$. The following choices of $z_{P,i}$ are compared: (1) $z_{1:2,1,1}^{(3)}$; (2) $z_{1:2,1,1}^{(2)}$; (3) $z_{1:2,1,1}^{(1)}$; (4) $z_{1:16,1,1}^{(3)}$; (5) $z_{1:4,1:2,1:2}^{(2)}$; (6) $z_{1:4,1:2,1:2}^{(1)}$; (7) $z_{1:48,1:2,1:2}^{(3)}$; (8) $z_{1:12,1:4,1:4}^{(2)}$; and (9) $z_{1:3,1:8,1:8}^{(1)}$.

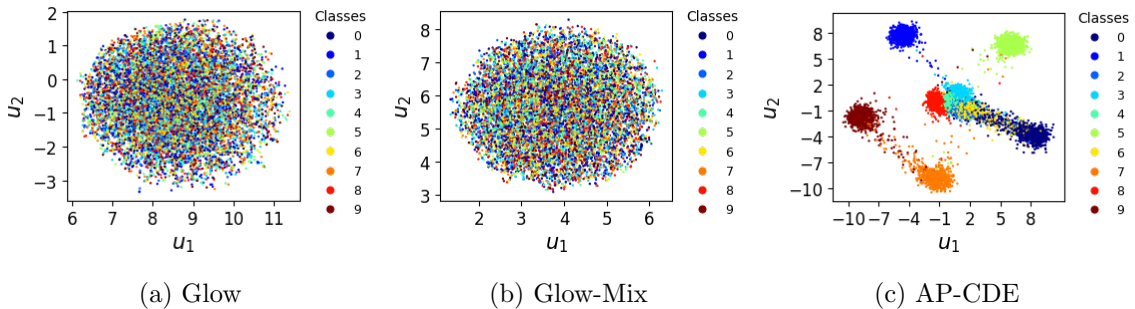


Figure 2: Latent representations estimated by the three models applied on the FashionMNIST training set. For the Glow and the Glow-Mix models, UMAP is used to reduce the dimensions to 2.

Figure 2 plots the latent representations produced by Glow, Glow-Mix and AP-CDE

with the choice (1) for the $z_{P,i}$. Recall that for Glow and Glow-Mix, the latent z_i has the same dimensionality as the images, UMAP (McInnes et al., 2018) is used to reduce the dimension and plot its output in 2D. For AP-CDE, the plot of the latent $z_{P,i}$ is provided. As expected, the latent variable produced by Glow follows a simple spherical Gaussian, and thus is not interpretable. Somewhat surprising, Glow-Mix does not produce a meaningful result either, despite using a mixture of 10 Gaussians (that corresponds to the true number of classes)—instead, the Glow-Mix model converges to only one component containing a mixture of z_i ’s from all classes. This negative finding is in accordance to an early critique on clustering with deep neural networks (Haeffele et al., 2020), where it was reported that in an unsupervised setting, imposing a modeling structure on the latent variable (such as a mixture of Gaussians) does not lead to a clear separation of data from different classes. Using AP-CDE and the supervising label information from x_i , we obtain a good separation of the ten products based on the low-dimensional representation $z_{P,i} \in \mathbb{R}^2$ for the model $z_{1:2,1,1}^{(3)}$ (shown in Figure 2(c)).

Table 1: The averages of bits per dimension on the training and the testing sets of FashionMNIST for all models. Lower BPM means higher density.

Models	Glow	Glow-Mix	Glow-CDE	Glow-NCDE	AP-CDE
Training set	1.02	1.04	1.03	1.31	1.02
Testing set	1.03	1.05	1.04	1.32	1.03

Table 1 depicts the average bits per dimension (BPM) on the training and the testing sets for all models. Here the BPM is the negative log-densities divided by the number of dimensions, which is broadly used in the literature because it has similar scale for different resolution of images. For AP-CDE model, we choose the best model considering the error rate and the density estimation performance among the all choices of $z_{P,i}$. The model of using $z_{1:48,1:2,1:2}^{(3)}$ is chosen. Clearly, for this dataset, AP-CDE, likely due to a better group-wise concentration, produces overall higher (or equal) marginal densities compared to its competitors.

Table 2 depicts the average bits per dimension on the training and the testing sets for all AP-CDE models as well as the classification error rates on the testing set, where one obtains $z_{P,i}$ and predict the label via the trained logistic regression model using $\arg \max_{k \in \{0, \dots, 9\}} f_{x|z_P}(k | T_{\hat{\theta}}^P(y_i))$. It shows that when one chooses more dimensions of the same level for the $z_{P,i}$, the classification error rate will be lower, while the density estimation performances do not vary significantly. Moreover, even when the $z_{P,i}$ has the same number of dimensions, the higher level can provide more accurate classification. This bunch of experiments is an important guidance on how to choose the dimensions for $z_{P,i}$ —the whole output of the last level is always not a bad choice.

Empirically it shows that the low-dimensional representation $z_{P,i}$ contains almost all the information to separate the different classes when the dimensions of $z_{P,i}$ are well chosen.

Table 2: The averages of bits per dimension on the training and the testing sets and the classification error rates on the testing sets for all AP-CDE models on the FashionMNIST data.

	$z_{1:2,1,1}^{(3)}$	$z_{1:2,1,1}^{(2)}$	$z_{1:2,1,1}^{(1)}$	$z_{1:16,1,1}^{(3)}$	$z_{1:4,1:2,1:2}^{(2)}$
BPM (Training set)	1.02	1.03	1.01	1.05	1.06
BPM (Testing set)	1.03	1.03	1.02	1.06	1.06
Error rate (%)	50.96	60.53	89.69	6.89	7.48

	$z_{1:4,1:2,1:2}^{(1)}$	$z_{1:48,1:2,1:2}^{(3)}$	$z_{1:12,1:4,1:4}^{(2)}$	$z_{1:3,1:8,1:8}^{(1)}$
BPM (Training set)	1.02	1.02	1.04	1.01
BPM (Testing set)	1.02	1.03	1.05	1.02
Error rate (%)	80.33	6.46	7.26	89.9

For the model $z_{1:48,1:2,1:2}^{(3)}$, as described in Section 3.2, if one fixes $z_{P,i}$, but replaces $z_{N,i}$ with independently sampled realizations from a Gaussian distribution, and then through $T_{\hat{\theta}}^{-1}$ one can obtain 10 new images for each original observation i . We then employ the ResNet101 (He et al., 2016) (a convolutional neural network separately trained on the training set) to classify these artificially generated images, and find that 95.26% of them are still classified to the same class label as the y_i 's. Hence, it is concluded that the $z_{N,i}$ largely corresponds to within-class variation, whereas $z_{P,i}$ captures between-class variation.

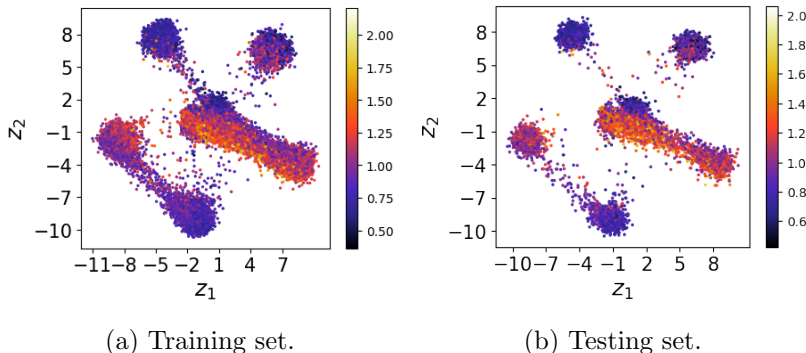


Figure 3: The first two dimensions of the latent variables from AP-CDE model $z_{1:2,1,1}^{(3)}$ on FashionMNIST, colored by the estimated densities in the scale of BPM.

Further, we color the latent $z_{P,i}$ using the magnitude of the density (Figure 3). In the result, those points with relatively low density values tend to correspond to images of low quality or higher ambiguity regarding the product class. To show this, we plot a few sampled fashion products in Figure 4 and sort each row by the density value in increasing

order. It can be seen that the images on the left tend to be harder to assign to a class, compared to the ones on the right.



Figure 4: Sample images from the AP-CDE model $z_{1:48,1:2,1:2}^{(3)}$ trained by FashionMNIST data, with each row sorted in the increasing order of estimated densities.

4.2 Human Face Photos

To illustrate the AP-CDE with continuous and mixed-type x_i , experiments are also run on the Yale face dataset. There are 2,414 face photos, each containing a single color channel with a 168×192 pixel resolution. The images are resized to 28×32 to reduce computation cost, while maintaining clarity of the photos. The images come from 38 people, and this information is used as a discrete class variable $x_{A,i}$. Further, the photos were taken under different light conditions, recorded as azimuth angle and elevation. This information is used as two continuous variables $x_{B,i}$ and $x_{C,i}$.

For the Glow model, the parameters are set to $L = 3$ and $K = 32$. A logistic regression likelihood $f_{x_A|z_{P_A}}$ is used for the discrete x_A , that depends on 3 dimensions of $z_{1:3,1,1}^{(3)}$. Here, $z^{(3)}$ is the output from the third level. Linear regression $x_{B,i} = \beta_0^B + \beta_1^B z_{P_B,i} + \epsilon_i^B$, $x_{C,i} = \beta_0^C + \beta_1^C z_{P_C,i} + \epsilon_i^C$ are employed for the other two covariates, where both $z_{P_B,i} = z_{4,1,1}^{(3)}$ and $z_{P_C,i} = z_{5,1,1}^{(3)}$ are one dimensional. Assume $\epsilon_i^B \stackrel{iid}{\sim} N(0, 0.01)$ and $\epsilon_i^C \stackrel{iid}{\sim} N(0, 0.01)$; note the low value of the variance selected, which forces higher correlation between (x_A, z_{P_A}) and

(x_B, z_{P_B}) . In this case, the last integral in Equation (2) has closed form because the integrand is the product of two Gaussian densities. The integral is $1/\sqrt{2\pi(\beta_2^2 + \beta_1^2)} \exp\{-(x_i - \beta_0)^2/[2(\beta_2^2 + \beta_1^2)]\}$.

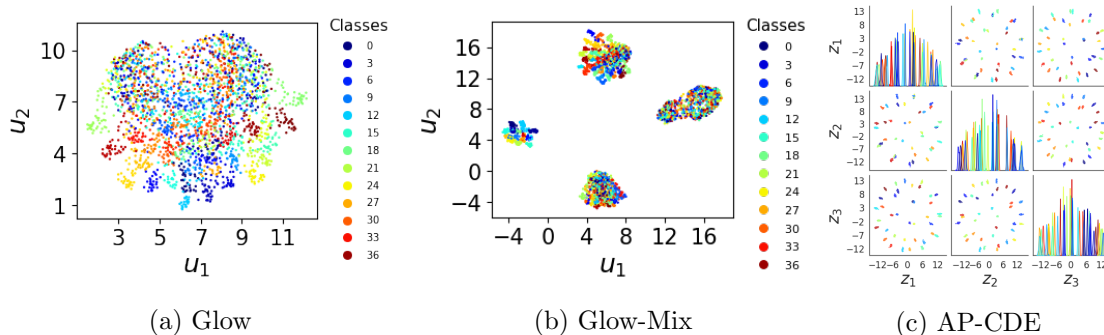


Figure 5: The latent representations estimated from the Yale face data. The UMAP is used to reduce the dimensions to 2 for Glow and Glow-Mix. For the AP-CDE model, all the dimensions of z_P are shown in pairs plot.

Competing methods include Glow and Glow-Mix. As can be seen in Figure 5, AP-CDE leads to a clear separation of latent representations due to the use of label information, whereas unsupervised Glow and Glow-Mix fail to do so. Further, the Glow model does not produce a group-mixed sphere as did in the FashionMNIST experiment. The Glow-Mix model produces four clusters in the latent space but none of them represents some class of people.

To show the expressiveness of AP-CDE as a generative model, the following procedure is used to synthesize new artificial images. One selects a range for Azimuth angles (-100 to 100) and a range for elevations (-60 to 60) (with interpolation), and form a 12×12 grid. For each grid cell, one draws a $Z_{P_A,i}$ that corresponds to a person’s identity, from the empirical posterior distribution from the AP-CDE estimates. Further, one randomly draws the $Z_{N,i}$ component from a $N(\vec{0}, I)$ distribution. With this choice of \tilde{z}_i , we synthesize new images for the i -th subject $\tilde{y}_i = T_{\hat{\theta}}^{-1}(\tilde{z}_i)$. As shown in Figure 6, there is a clear trend of change in the lighting conditions, caused by the changing values of $(x_{B,i}, x_{C,i})$.

5 Data Application

In the application study, we use 18001 images of leaves from strawberry plants, which either are healthy or have one of the three types of diseases: powdery mildew, anthracnose and fusarium wilt. This forms the labels of the four classes, which can be treated as the predictor variable x . The AP-CDE model is expected to conditionally estimate the densities of the images as well as do a supervised dimensional reduction.

Considering that the backgrounds of the images cause overfitting problem because the similarities between backgrounds rather than between the characteristics of the diseases take

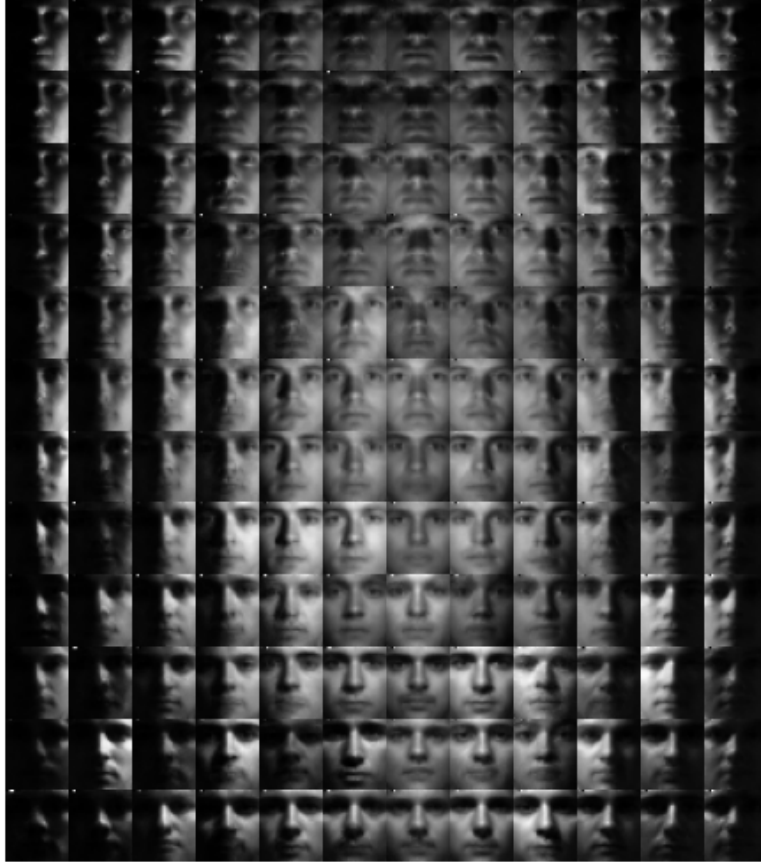


Figure 6: Synthesized face photos with gradually changing light azimuth angles (left to right) and elevations (top to bottom).

account for the major contribution on the distinction of the several groups (Saikawa et al., 2019), we use the method mentioned in Saikawa et al. (2019) to remove the backgrounds of all images. This segmentation also enhanced the quality of density estimation by reducing the redundant information. The images are resized to 128×128 resolution. To improve visual quality in generating samples, we follow Kingma and Dhariwal (2018) to use 5-bit images. Then they dequantize the pixel values as stated in the Section 4. The data is split into training set which includes 16000 images and the testing set which includes 2001 images.

For the parameters of Glow, the parameters are set to $L = 6$ and $K = 32$. For the conditional likelihood of $x | z_P$, again, we use $f_{x|z} \propto g_{x|z}^\lambda$, where g is the likelihood function of the multinomial logistic regression through the origin and $\lambda = 1000$. The subvector $z_{P,i}$ is chosen to be the output of the last level, which has dimension $384 \times 2 \times 2$.

Table 3 shows the average bits per dimension results for all models on the training and

Table 3: The averages bits per dimension on the training and the testing sets of the leaves of strawberry plants data for all models.

Models	Glow	Glow-Mix	Glow-CDE	Glow-NCDE	AP-CDE
Training set	4.16	4.25	4.19	4.18	4.16
Testing set	4.17	4.26	4.22	4.18	4.17

testing sets. The proposed AP-CDE model outperforms the other competitors on density estimation, while gets results as good as Glow. Figure 8(b) shows generated images for each of the four classes. As a comparison, Figure 8(a) shows the real images for each of the four classes. The second column shows the generated powdery mildew images, which clearly have some white spots on the leaves; the third column shows the generated anthracnose images, which have purple spots on the leaves; and the fourth column shows the generated fusarium wilt images.

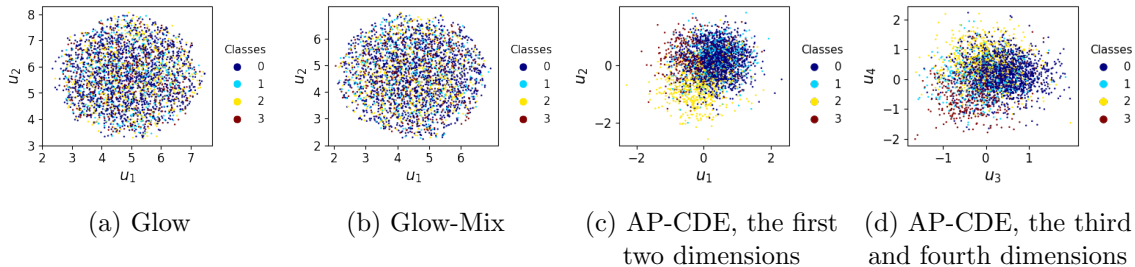
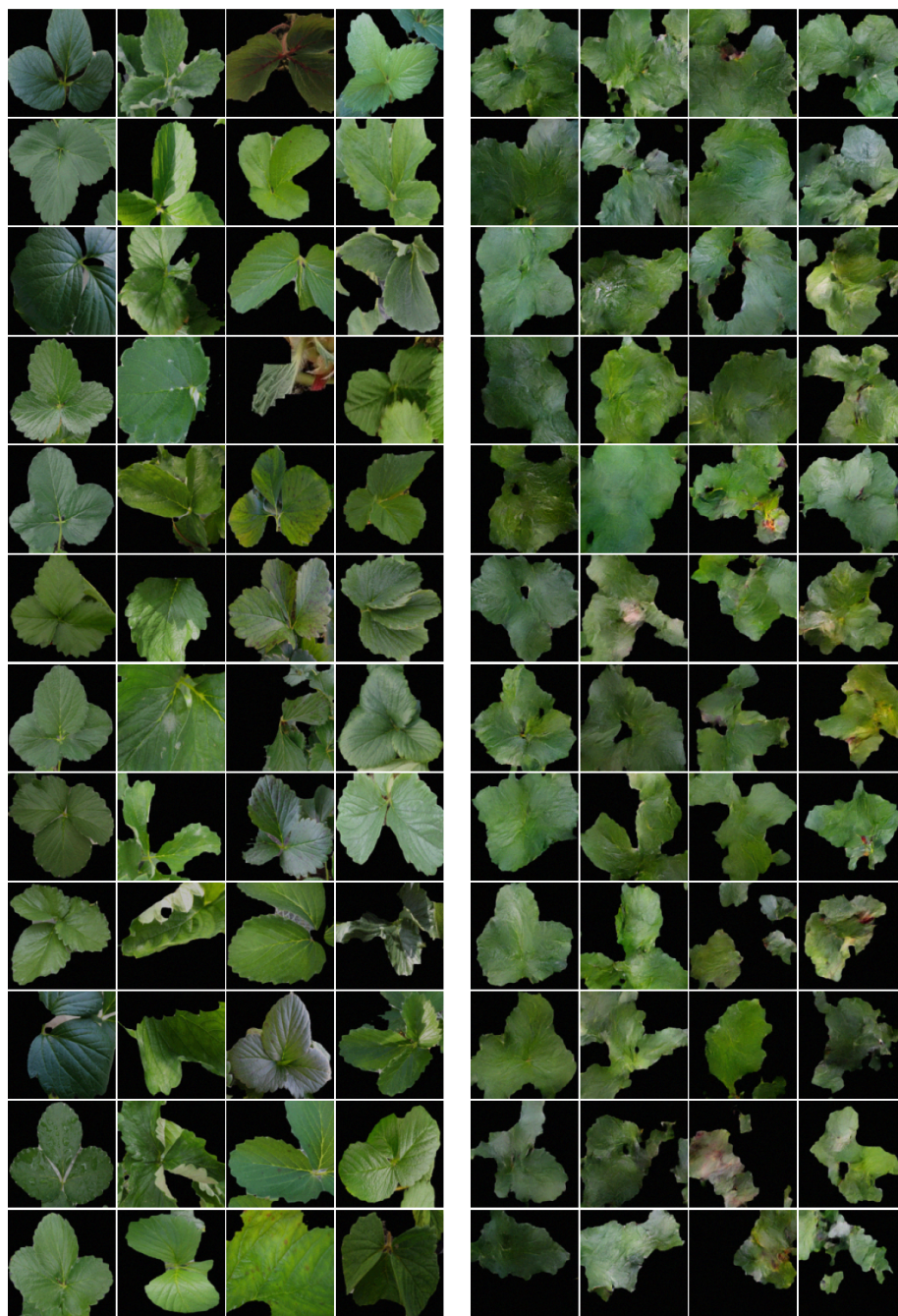


Figure 7: The latent variables mapping from the leaves of strawberry plants images produced from the models. The UMAP is used to reduce the dimensions to 2 for Glow and Glow-Mix models.

For this complex dataset, the proposed model still captures some features of the diseases of the strawberry plants, and gives 20.8% classification error on the testing set, where the label is predicted via the logistic regression model on the $z_{P,i}$. We also validate the model using the method stated in Section 3.2 and the independent classification model for which the ResNet101 is used gets 82.7% accuracy on the new generated images. This means the AP-CDE model is helpful for conditional generating more images of leaves of strawberry plants. Figure 7 plots the latent representations produced by these models. For Glow and Glow-Mix, the UMAP (McInnes et al., 2018) is used to reduce the dimension of latent z_i and plot its output in 2D. For the latent $z_{P,i}$ produced by AP-CDE, the plot between the first and the second dimension is provided, as well as the plot between the third and the fourth dimension. The Glow and Glow-Mix models do not provide any useful dimension reduction, while the latent variables provided by AP-CDE are separated over the four classes.



(a) Real images

(b) Generated images

Figure 8: Real images and generated images using the AP-CDE model for the leaves of strawberry plants.

6 Discussion

We extend the normalizing flow neural network to the task of CDE. It produces a generative model for high-dimensional data that can incorporate information from external predictors. Importantly, by using only a subset of the one-to-one transform from the high-dimensional data, a useful dimension reduction is achieved, in which the low-dimensional representation is empirically sufficient to characterize the changes of the response variable due to the predictor.

A number of neural network-based models for CDE have appeared in the literature (see, e.g., recent reviews Ambrogioni et al. (2017); Rothfuss et al. (2019)). Nevertheless, we want to emphasize the versatility and simplicity of the proposed approach. AP-CDE can work with any existing normalizing flow network architecture, with only a modification of the base distribution density from a normal one to the product of a prior distribution and a likelihood function.

There are several interesting directions for future work. First, there is a connection of the strategy for new photo synthesis—“keeping z_P , sampling \tilde{z}_N and pulling back via T^{-1} ”—to the popular practice of “data augmentation in deep learning” (Shorten and Khoshgoftaar, 2019). Conventionally, to counter the small training sample problem, especially in image modeling, one relies on techniques such as geometric transformations, color space augmentation and random erasing. Nevertheless, there is a recent trend in using another neural network for data augmentation, such as adversarial training and neural style transfer. The proposed AP-CDE can be considered another solution. Second, the normalizing flow networks can be too flexible, in the sense that they could transform a data distribution approximately to *any* latent distribution. This is likely why the unsupervised mixture of Gaussian latent distribution fails to explain the variations in the observed space. The proposal of using the predictor-conditional distribution shows that there is room to make the latent variable more interpretable; nevertheless, caution should be taken and additional validation methods could be developed.

References

- Luca Ambrogioni, Umut Güçlü, Marcel AJ van Gerven, and Eric Maris. The kernel mixture network: A nonparametric method for conditional density estimation of continuous random variables. *arXiv:1705.07111*, 2017.
- Jens Behrmann, Will Grathwohl, Ricky TQ Chen, David Duvenaud, and Jörn-Henrik Jacobsen. Invertible residual networks. In *International Conference on Machine Learning*, pages 573–582. PMLR, 2019.
- Mikhail Belkin and Partha Niyogi. Laplacian eigenmaps for dimensionality reduction and data representation. *Neural Computation*, 15(6):1373–1396, 2003.

- Zdravko I Botev, Joseph F Grotowski, and Dirk P Kroese. Kernel density estimation via diffusion. *The Annals of Statistics*, 38(5):2916–2957, 2010.
- Noirrit Kiran Chandra, Antonio Canale, and David B Dunson. Escaping the curse of dimensionality in Bayesian model-based clustering. *Journal of machine learning research*, 24(144):1–42, 2023.
- Ricky TQ Chen, Jens Behrmann, David K Duvenaud, and Jörn-Henrik Jacobsen. Residual flows for invertible generative modeling. *Advances in Neural Information Processing Systems*, 32, 2019.
- Hugh A Chipman, Edward I George, and Robert E McCulloch. Bart: Bayesian additive regression trees. *The Annals of Applied Statistics*, 4(1):266–298, 2010.
- R Dennis Cook and Liqiang Ni. Sufficient dimension reduction via inverse regression: A minimum discrepancy approach. *Journal of the American Statistical Association*, 100(470):410–428, 2005.
- Laurent Dinh, Jascha Sohl-Dickstein, and Samy Bengio. Density estimation using real NVP. *arXiv:1605.08803*, 2016.
- Chris Fraley and Adrian E Raftery. Model-based clustering, discriminant analysis, and density estimation. *Journal of the American Statistical Association*, 97(458):611–631, 2002.
- Ashutosh Garg and Dan Roth. Understanding probabilistic classifiers. In *European Conference on Machine Learning*, pages 179–191. Springer, 2001.
- Alan E Gelfand. Gibbs sampling. *Journal of the American Statistical Association*, 95(452):1300–1304, 2000.
- Mathieu Germain, Karol Gregor, Iain Murray, and Hugo Larochelle. Made: Masked auto-encoder for distribution estimation. In *International Conference on Machine Learning*, pages 881–889. PMLR, 2015.
- John Geweke and Michael Keane. Smoothly mixing regressions. *Journal of Econometrics*, 138(1):252–290, 2007.
- Will Grathwohl, Ricky TQ Chen, Jesse Bettencourt, Ilya Sutskever, and David Duvenaud. Ffjord: Free-form continuous dynamics for scalable reversible generative models. *arXiv:1810.01367*, 2018.
- Peter Grünwald and Thijs Van Ommen. Inconsistency of Bayesian inference for misspecified linear models, and a proposal for repairing it. *Bayesian Analysis*, 12(4):1069–1103, 2017.
- Benjamin D Haeffele, Chong You, and René Vidal. A critique of self-expressive deep subspace clustering. *arXiv:2010.03697*, 2020.

- Kaiming He, Xiangyu Zhang, Shaoqing Ren, and Jian Sun. Deep residual learning for image recognition. In *Proceedings of the IEEE conference on computer vision and pattern recognition*, pages 770–778, 2016.
- Ziyi Huang, Henry Lam, and Haofeng Zhang. Evaluating aleatoric uncertainty via conditional generative models. *arXiv:2206.04287*, 2022.
- Pavel Izmailov, Polina Kirichenko, Marc Finzi, and Andrew Gordon Wilson. Semi-supervised learning with normalizing flows. In *International Conference on Machine Learning*, pages 4615–4630. PMLR, 2020.
- Wenxin Jiang and Martin A Tanner. Hierarchical mixtures-of-experts for exponential family regression models: Approximation and maximum likelihood estimation. *The Annals of Statistics*, 27(3):987–1011, 1999.
- JooSeuk Kim and Clayton D Scott. Robust kernel density estimation. *Journal of Machine Learning Research*, 13(1):2529–2565, 2012.
- Diederik P Kingma and Jimmy Ba. Adam: A method for stochastic optimization. *arXiv:1412.6980*, 2014.
- Durk P Kingma and Prafulla Dhariwal. Glow: Generative flow with invertible 1x1 convolutions. *Advances in Neural Information Processing Systems*, 31, 2018.
- Yi-Hung Kung, Pei-Sheng Lin, and Cheng-Hsiung Kao. An optimal k-nearest neighbor for density estimation. *Statistics & Probability Letters*, 82(10):1786–1791, 2012.
- Neil Lawrence. Gaussian process latent variable models for visualisation of high dimensional data. *Advances in Neural Information Processing Systems*, 16, 2003.
- Kuang-Chih Lee, Jeffrey Ho, and David J Kriegman. Acquiring linear subspaces for face recognition under variable lighting. *IEEE Transactions on Pattern Analysis and Machine Intelligence*, 27(5):684–698, 2005.
- Ilya Loshchilov and Frank Hutter. Sgdr: Stochastic gradient descent with warm restarts. *arXiv:1608.03983*, 2016.
- YP Mack and Murray Rosenblatt. Multivariate k-nearest neighbor density estimates. *Journal of Multivariate Analysis*, 9(1):1–15, 1979.
- Leland McInnes, John Healy, and James Melville. Umap: Uniform manifold approximation and projection for dimension reduction. *arXiv:1802.03426*, 2018.
- Geoffrey J McLachlan and David Peel. Mixtures of factor analyzers. In *Proceedings of the seventeenth international conference on machine learning*, pages 599–606, 2000.

- Eric Nalisnick, Akihiro Matsukawa, Yee Whye Teh, Dilan Gorur, and Balaji Lakshminarayanan. Hybrid models with deep and invertible features. In *International Conference on Machine Learning*, pages 4723–4732. PMLR, 2019.
- Andriy Norets. Approximation of conditional densities by smooth mixtures of regressions. *The Annals of Statistics*, 38(3):1733–1766, 2010.
- George Papamakarios, Theo Pavlakou, and Iain Murray. Masked autoregressive flow for density estimation. *Advances in Neural Information Processing Systems*, 30, 2017.
- George Papamakarios, Eric T Nalisnick, Danilo Jimenez Rezende, Shakir Mohamed, and Balaji Lakshminarayanan. Normalizing flows for probabilistic modeling and inference. *Journal of Machine Learning Research*, 22(57):1–64, 2021.
- Xi Peng, Jiashi Feng, Joey Tianyi Zhou, Yingjie Lei, and Shuicheng Yan. Deep subspace clustering. *IEEE Transactions on Neural Networks and Learning Systems*, 31(12):5509–5521, 2020.
- Jonas Rothfuss, Fabio Ferreira, Simon Walther, and Maxim Ulrich. Conditional density estimation with neural networks: Best practices and benchmarks. *arXiv:1903.00954*, 2019.
- Sam T Roweis and Lawrence K Saul. Nonlinear dimensionality reduction by locally linear embedding. *Science*, 290(5500):2323–2326, 2000.
- Takumi Saikawa, Quan Huu Cap, Satoshi Kagiwada, Hiroyuki Uga, and Hitoshi Iyatomi. Aop: An anti-overfitting pretreatment for practical image-based plant diagnosis. In *2019 IEEE International Conference on Big Data (Big Data)*, pages 5177–5182. IEEE, 2019.
- John W Sammon. A nonlinear mapping for data structure analysis. *IEEE Transactions on Computers*, 100(5):401–409, 1969.
- Bernhard Schölkopf, Alexander Smola, and Klaus-Robert Müller. Kernel principal component analysis. In *International Conference on Artificial Neural Networks*, pages 583–588. Springer, 1997.
- Erich Schubert, Arthur Zimek, and Hans-Peter Kriegel. Generalized outlier detection with flexible kernel density estimates. In *Proceedings of the 2014 SIAM International Conference on Data Mining*, pages 542–550. SIAM, 2014.
- David W Scott. Partial mixture estimation and outlier detection in data and regression. In *Theory and Applications of Recent Robust Methods*, pages 297–306. Springer, 2004.
- Connor Shorten and Taghi M Khoshgoftaar. A survey on image data augmentation for deep learning. *Journal of Big Data*, 6(1):1–48, 2019.

- Liangjun Su and Halbert White. A consistent characteristic function-based test for conditional independence. *Journal of Econometrics*, 141(2):807–834, 2007.
- Liangjun Su and Halbert White. A nonparametric hellinger metric test for conditional independence. *Econometric Theory*, 24(4):829–864, 2008.
- Yichuan Tang, Ruslan Salakhutdinov, and Geoffrey Hinton. Deep mixtures of factor analyzers. *arXiv:1206.4635*, 2012.
- George R Terrell and David W Scott. Variable kernel density estimation. *The Annals of Statistics*, pages 1236–1265, 1992.
- Michael E Tipping and Christopher M Bishop. Mixtures of probabilistic principal component analyzers. *Neural Computation*, 11(2):443–482, 1999.
- Laurens Van der Maaten and Geoffrey Hinton. Visualizing data using t-sne. *Journal of Machine Learning Research*, 9(11), 2008.
- Mattias Villani, Robert Kohn, and Paolo Giordani. Regression density estimation using smooth adaptive gaussian mixtures. *Journal of Econometrics*, 153(2):155–173, 2009.
- Han Xiao, Kashif Rasul, and Roland Vollgraf. Fashion-MNIST: A novel image dataset for benchmarking machine learning algorithms. *arXiv:1708.07747*, 2017.
- Konstantin M Zuev, James L Beck, and Lambros S Katafygiotis. On the optimal scaling of the modified Metropolis–Hastings algorithm. In *Proceedings of 11th international conference on applications of statistics and probability in civil engineering (ICASP2011)*, pages 1–4, 2011.

A MNIST Handwritten Digit Images

In this section, additional experiment results are shown using the MNIST data.

The MNIST data is used to illustrate the CDE when x is discrete. This dataset contains 70,000 processed images of handwritten digits, each having 28×28 pixels. We use 60,000 for training purposes and the remaining for testing. Each image y_i is associated with a discrete label x_i recording the ground-truth digit from 0 to 9.

The structure of this dataset is very similar to FashionMNIST (Xiao et al., 2017) which is used in the main paper, and the same models as in Section 3.1 is used. The latent $z_{P,i}$ is chosen to be $z_{1:16,1,1}^{(3)}$. Unsurprisingly, the results corresponding to this dataset is quite similar to the ones from the FashionMNIST dataset.

Figure 9 plots the latent representations produced by Glow, Glow-Mix and AP-CDE. For AP-CDE, the latent $z_{1:2,1,1}^{(3)}$ is used as the $z_{P,i}$ for a better illustration in two dimensional reduction. For Glow and Glow-Mix, the UMAP (McInnes et al., 2018) is used to reduce the

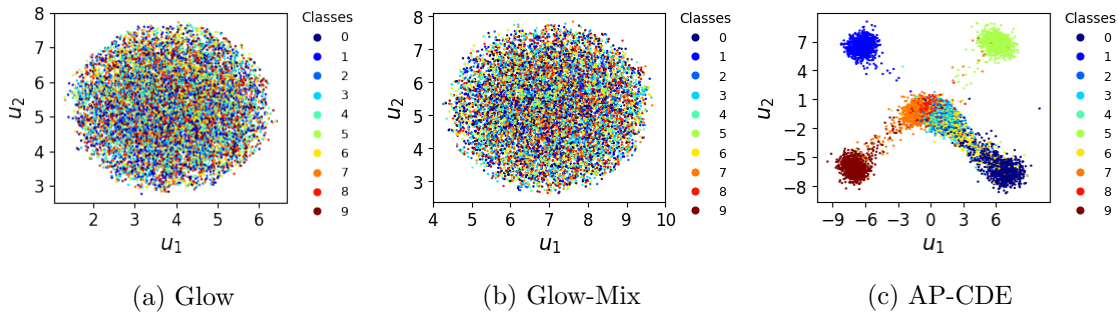


Figure 9: Latent representations estimated by three models applied on the MNIST training set. For Glow and Glow-Mix models, since the latent are in high dimensions, the UMAP is used to reduce the dimensions to 2. Neither of them produces interpretable latent presentations, whereas AP-CDE model does the latent that can be easily separated into groups.

dimension and plot its output in 2D. For AP-CDE, the latent $z_{P,i}$ is provided. As expected, the latent variable produced by Glow follows a simple spherical Gaussian, and thus is not interpretable. The Glow-Mix does not produce a meaningful result either. Using AP-CDE and the supervising label information from x_i , we obtain a good separation of the ten digits based on the low-dimensional representation $z_{P,i} \in \mathbb{R}^2$ (shown in Figure 9(c)).

Under the working model using $z_{1:16,1,1}^{(3)}$ as $z_{P,i}$, for the testing set, we obtain $z_{P,i}$ and predict the label via the trained logistic regression model [using $\arg \max_{k \in \{0, \dots, 9\}} f_{x|z_P}(k | T_{\hat{\theta}}^P(y_i))$] to obtain classification accuracy of 98.5%. Empirically it is shown that the low-dimensional representation $z_{P,i}$ contains almost all the information to separate the different classes. As described in Section 3.1, we employ the ResNet101 to classify the artificially generated images from the proposed AP-CDE model with fixed $z_{P,i}$'s, and find that 96.14% of them are still classified to the same class label as the y_i 's. Hence, it is concluded that the $z_{N,i}$ largely corresponds to within-class variation, whereas $z_{P,i}$ captures between-class variation.

Table 4: The averages of the bits per dimension on the training and the testing sets of MNIST data.

Models	Glow	Glow-Mix	Glow-CDE	Glow-NCDE	AP-CDE
Training set	1.01	1.02	1.03	1.23	1.01
Testing set	1.01	1.03	1.04	1.28	1.01

As seen in Figure 9(c), x_i tends to make each group of z_i 's (each group corresponding to a digit) more concentrated to their respective center, which leads us to compare the marginal densities $f_y(y_i)$ with the ones from competing methods. Table 4 depicts the average of the log-densities on the training and the testing sets for all models. Clearly, for this dataset, AP-CDE, likely due to a better group-wise concentration, produces overall higher or not

lower marginal densities compared to its competitors. Note that bits per dimension is the negative log density over the number of dimensions.

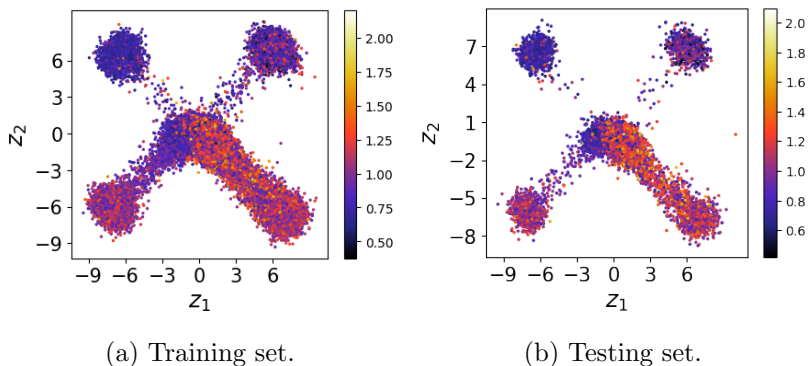


Figure 10: The first two dimensions of the latent variables from AP-CDE, colored by the estimated densities in the scale of bits per dimension.

Further, the latent $z_{P,i}$ is colored using the magnitude of the bits per dimension (Figure 10). In the result, those points with relatively high BPM values (low density values) tend to correspond to images of low quality or higher ambiguity regarding the digit class. The easier classified classes have relatively higher densities. To show this, we plot a few sampled digits in Figure 11 and sort each row by the density value in increasing order. It can be seen that the images on the left tend to be harder to assign to a class, compared to the ones on the right.



Figure 11: Sample images from the MNIST data, with each row sorted in the increasing order of estimated densities.